Construction and Building Materials 305 (2021) 124681

Contents lists available at ScienceDirect

Construction and Building Materials

journal homepage: www.elsevier.com/locate/conbuildmat

Durability of an UHPC containing spent equilibrium catalyst

Ana Mafalda Matos [a], Sandra Nunes [a,*], Carla Costa [b], José L. Barroso Aguiar [c]

[a] CONSTRUCT-LABEST, Department of Civil Engineering, Faculty of Engineering, University of Porto, Porto, Portugal
[b] High Institute of Engineering of Lisbon (ISEL), Lisbon Polytechnic Institute, Portugal
[c] Department of Civil Engineering, University of Minho, Centro de Território, Ambiente e Construção, Guimarães, Portugal

ARTICLE INFO

Keywords:
Ultra-high performance fibre reinforced cementitious composites (UHPFRC)
Spent equilibrium catalyst (ECat)
By-product valorisation
Porosity
Capillary water absorption
Chloride migration
Alkali-silica reaction
Sulphate attack

ABSTRACT

UHPC is an advanced cementitious material able to meet the current construction industry challenges regarding structural safety and durability. However, new UHPC formulations with limited shrinkage are still being pursued to reduce residual tensile stresses in the UHPFRC layers, for rehabilitation/strengthening applications. This investigation estimates the durability of a non-proprietary UHPC incorporating a by-product originated by the oil refinery industry (ECat), as an internal curing agent. Direct and indirect transport properties measurements as well as the carbonation assessment and evaluation of dimensional resilience to potential deleterious reactions revealed that the new UHPC possesses an excellent durability performance, typical of these materials. These results combined with its self-compacting ability, low autogenous shrinkage and high compressive strength confirm the belief in the role of this new UHPC towards a high-tech construction.

1. Introduction

The construction sector bears a heavy social and environmental responsibility to ensure that society has sufficient concrete to satisfy its future needs while also lowering the energy consumption, dioxide carbon emissions, exploitation of natural resources and wastes generation. Furthermore, it can provide a solution for a variety of industrial by-products and wastes that can enter a new lifecycle, preventing dumping and landfilling, and therefore serving as an ally regarding the Circular Economy objective.

Over the last decades, considerable efforts to improve the behaviour of cementitious materials led to the emergence of the ultra-high performance fibre reinforced cementitious composites (UHPFRC). The key principles for designing UHPFRC are in porosity decreasing and toughness increasing that is associated to microstructure improvement and homogeneity enhancement. The raw materials (chemical–mineralogical nature and content level), including the fibres, as well as the curing regimes, are the main factors that determine both the outstanding mechanical and durability performances of UHPFRC [1–8].

Traditional UHPFRC is a mixture of powder materials with a maximum particle size of 1 mm. The binder materials include a high proportion of cement (800–1000 kg/m^3) and reactive powder materials, like silica fume (SF), ground granulated blast furnace slag (GGBFS), fly ash (FA), metakaolin (MTCK), rice husk ash (RHA), among others [1]. The water to binder mass ratio (w/b) is often below 0.20. Consequently, a high content of superplasticizer on polycarboxylate ether basis is necessary (in general, 1.4–2.4 % by cement weight) [2]. Fibres used in UHPFRC are typically short high-strength steel fibres, which allow incorporating a significant volume of fibres (V_f), ranging from 2 to 4%. Besides, the use of special curing treatments (such as heat treatment, autoclave or steam curing and pressure) accelerates the UHPFRCs' hydration process and increases their density also contributing to the ultra-high compressive strengths. Owing to its dense microstructure, UHPC is highly susceptible to explosive spalling and severe damage when subjected to high temperature [9]. The steel fibres alone cannot prevent the occurrence of explosive spalling under fire conditions but adding synthetic fibres (like polyvinyl alcohol fibres and a combination of polypropylene and nylon fibres) was found to be effective to enhance the UHPFRC fire resistance [10].

Major applications of UHPFRC in new structures constitute factory precast elements assembled on-site namely slender and lightweight elements for pedestrian footbridges and highway bridges, or to build structures with specific architectural or aesthetic requirements [11]. Typically, UHPFRC on-site production is only carried out for rehabilitation and strengthening purposes. In this regard, the key advantages of the UHPFRC is the limited volumes needed and its ability to perform a dual role (strengthening and water tightness) whilst requires short-term interventions [12]. Considering the high cost of some constituent materials and the complexity of the curing processes, the use of non-

* Corresponding author.
E-mail addresses: up200505574@fe.up.pt (A.M. Matos), snunes@fe.up.pt (S. Nunes), carla.costa@isel.pt (C. Costa), aguiar@civil.uminho.pt (J.L.B. Aguiar).

https://doi.org/10.1016/j.conbuildmat.2021.124681
Received 8 March 2021; Received in revised form 10 July 2021; Accepted 23 August 2021
Available online 8 September 2021

Nomenclature

List of abbreviations and symbols

ASR	Alkalis-silica reaction
BET	Brunauer–Emmett–Teller theory for the measurement of the specific surface area of materials
BSE	Backscattered electron mode (in scanning electron microscopy)
CH	Calcium Hydroxide
C-LDH	Calcined Layered Double Hydroxide
CSH	Calcium silicates hydrated
$CaCO_3$	Calcium carbonate
CO_2	Carbon dioxide
D_{nssm}	Non-steady-state migration coefficient
ECat	Equilibrium catalyst
FA	Fly ash
GGBFS	Ground granulated blast-furnace slag
LF	Limestone filler
LOI	Loss on ignition
MIP	Mercury intrusion porosimetry
MTCK	Metakaolin
Na_2Oeq	Alkali equivalent content
NaOH	Sodium hydroxide
PSD	Pore size distribution
RCM	Rapid chloride migration test
RH	Relative humidity (%)
RHA	Rice husk ash
RPC	Reactive powder concrete
SCM	Supplementary cementitious materials
SEM	Scanning electron microscopy
SF	Silica fume
Sp	Polycarboxylate-based superplasticizer
t	Delay time between casting of samples and initiation of a given curing stage (day/h)
T	Curing temperature (°C)
UHPC	Cementitious matrix of an UHPFRC
UHPFRC	Ultra-High Performance Fibre Reinforced Cementitious Composites
V_f	Volume of fibres (%)
w/c	water to cement mass ratio
w/b	water to binder mass ratio
XRF	X-ray fluorescence spectrometry
Δt	Duration of a given curing stage (day/h)

conventional materials (including, agricultural and other industrial residues), as well as, common technology, such as conventional casting and room temperature curing has been preferred by several authors in order to facilitate the production and applications of UHPFRC [13–17]. In addition, the introduction of coarse aggregate was also set as a strategy to reduce the binder content in UHPC, reducing its unit cost and making it more environmentally friendly [18–20]. Besides the SF that is a typical constituent of UHPFRC, other by-products that were already used as partial surrogates of cement or fine aggregate include FA [21,22], bottom ash [13], sugarcane bagasse ash [14], glass powder [15,16], RHA [17,23] and GGBFS [24,25].

Spent equilibrium catalyst (ECat) is a by-product originated in the fluid catalytic cracking (FCC) unit of the oil refinery industry. Although the data released by the refineries is scarce [26], the FCC catalyst consumption worldwide was ca. 600–840 metric kton (depending on the data source) in 2014 [27–29], and it is expected to grow in the forthcoming years [30]. The current scenario originates annually ca. 400 metric kton of ECat worldwide [31,32], of which about 2 kton originated by the Portuguese oil refinery industry. Since most of the ECat is disposed of in landfills [26,28], there is a keen interest to upgrade its reuse in high-value applications, such as hydraulic binders' constituents.

The ECat generated in Portugal proved to exhibit high pozzolanic reactivity (evaluated both through direct and indirect test methods) [33], similar to that of silica fume [34] and metakaolin [35]. Thus, it may be used as 10–20% (by mass) partial cement surrogate in mortars and concretes (vibrated and self-compacting) without impairing neither (early and long-term) the mechanical properties [35,36] nor the durability [33,37] of the final materials. Moreover, ECat is a highly microporous material with very high specific surface area (150 070 m^2/kg determined by BET), and exhibiting a significant water absorption capacity (30% by mass) [35]. A possible breakthrough can thus be sought in exploiting this by-product as an internal curing agent in UHPFRC, particularly in mixtures for rehabilitation/strengthening purposes that require low early-ages cracking risk and on-site fabrication under normal casting and curing conditions. Following this purpose, [34,38], the authors optimised a new non-proprietary UHPC mixture incorporating ECat originated in Portugal. In particular, this UHPC mixture was optimised to exhibit low autogenous shrinkage at early ages (mitigating the early-ages cracking risk) and to be durable (assessed through the highest electrical resistivity value at 28 days) without jeopardize neither the self-compatibility nor the compressive strength [34].

The current paper focuses on deepening the durability performance of this new non-proprietary UHPC, mentioned above. As such, a series of durability indicators (Section 4) were experimentally obtained and compared with results reported in the literature for both other non-proprietary and commercially-available UHPC materials. To achieve this objective, Section 2 presents a literature survey of the critical properties for the long-term performance of UHPC and discusses the influence of various material/curing parameters on the durability performance of UHPC. Section 3 reports the procedures used on the durability assessment tests performed on the new UHPC to assess its porosity, water absorption by capillarity, chloride ions penetrability and expansive reactions susceptibility. Section 5 systematizes the durability indicators obtained revealing that actually the developed UHPC with ECat incorporation has similar performance than the other UHPCs, under similar curing conditions.

2. Durability performance indicators of UHPC/UHPFRC

The majority of the deterioration processes in cement-based materials comprise the transport of the harmful substances (gases, liquids or ions) across their porous matrices. Thus, their durability assessment typically involves testing the porosity and transportation processes such as absorption, migration and diffusion. As such, the durability of the developed UHPC was estimated based on porosity, resistance to water and chloride ion ingress, as well as susceptivity to carbonation and expansive reactions. These are generally considered good indicators of whether a cement-based material will withstand the harsh environmental conditions in service. Thus, the current section assesses the previous conducted studies on UHPC/UHPFRC that evaluated one (or several) of these durability indicators.

Considering the novelty of UHPC/UHPFRC in the construction industry, a key point for upcoming investigations on newly developed materials is a statistical descriptive analysis of a comprehensive data collection of durability indicators obtained on similar products. A wide variety of data have been collected from a total of 42 research papers/reports, published between 1996 and 2020. The collected experimental studies have been evaluated regarding the durability properties, compressive strength level attained, curing regime and mix design of UHPC/UHPFRC. Summary of the collected data and presented

information are provided in Supplementary Tables S1 to S4.

2.1. Porosity

A typical pore size distribution (PSD) for hydrated cement matrices encompasses a broad range of pore sizes, from about nanometres to centimetres in diameter. The PSD and its degree of continuity are the most significant factors determining the transport properties of the cement matrix. Mercury intrusion porosimetry (MIP) is a major method used to characterise the pore structure of hydrated UHPC [39], regarding its total porosity and the critical pore diameters. In cement pastes, the highest critical pore diameter is generally assumed corresponding to the capillary porosity whereas the lowest critical pore diameter corresponding to the gel pores. A classification of potential durability is proposed in [40] based on porosity measured by MIP, shown in Table 1.

The Supplementary Table S1 summarises 103 results of MIP and compressive strength of UHPCs reported in literature considering the following influencing factors: binder composition, w/b ratio, curing regime and age. Fig. 1 shows the box-plot representation of 48 of those total porosity results obtained at 28 days (data from last column in Supplementary Table S1).

The Supplementary Table S1 shows that, as referred above, the reported UHPCs were prepared with very low w/b ratio (0.13–0.22) and with diverse binders' constituents, leading to high compressive strength (100–279 MPa) [13,21,22,41-52]. Their binder composition often consists of cement (different types) combined with one or more SCM types, namely, industrial wastes (such as, SF, GGBS, FA); calcined clays (metakaolin); vegetables ashes (such as, rice ash and bottom ash); and filler materials (such as, limestone filler, quartz powder). The effect of particles in the nano-size range was also considered, namely, nano-silica [46], nano-$CaCO_3$ [49], and carbon nanofibers [21]. The reported studies covered different curing regimes, namely, normal curing conditions and different curing time [48,50,53], thermal treatment [41,45] and autoclave curing conditions [22]. In brief, the actual effect of using SCM materials as cement or SF surrogates on the porosity of UHPC depends on different factors namely, the SCM chemical–mineralogical composition, particles size distribution and content as well as on hydration time of the UHPC. Both heat-treatment and autoclave pressure are effective to accelerate the densification of the UHPC matrices. In addition, it should be stressed that part of the variation found in MIP results reported in the literature might also be due to differences in the procedures used for samples preparation, measurement conditions and/or data analysis.

Considering the values represented in Fig. 1, the median, the 25th percentile and the 75th percentile of the dataset are 5%, 4% and 8%, respectively. Data points that lie outside the 10th and 90th percentiles are represented by dot symbols (the same applies for the remaining box-plots presented in this section). The middle 50 percent of the total porosity data found in the literature ranging from 4% to 8% (i.e. interval from the 25th to the 75th percentile), lies in the region where materials are considered to have "Very high"/"High" potential durability shown in Table 1.

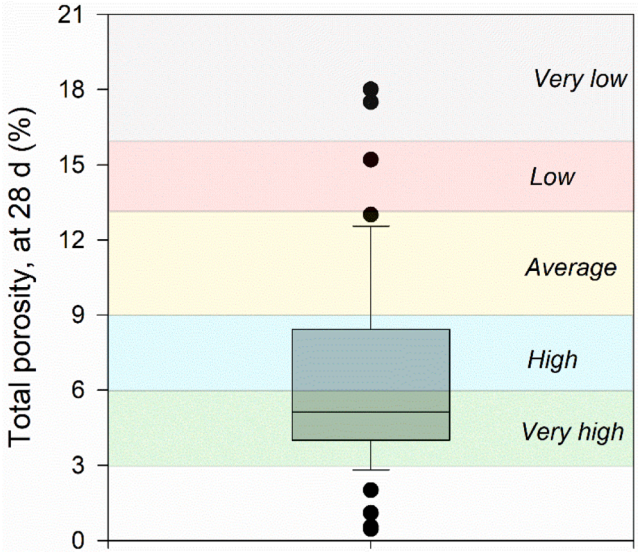

Fig. 1. Box-plot of total porosity data (28 days) reported in the literature and potential durability classification (as proposed in [40]).

2.2. Water absorption by capillarity

Sorptivity is other key parameter for assessing durability of cementitious materials indicating how easily moisture containing harmful agents can penetrate through the concrete cover porosity by capillary absorption. The RILEM's technical committee for performance-based specifications and control of concrete durability (RILEM TC 230-PSC) [54] set a classification for concrete quality considering water sorptivity at 28 days presented in Table 2.

Supplementary Table S2 summarizes 65 results of capillary water absorption obtained on UHPC/UHPFRC reported in literature considering binder composition, fibre volume, w/b ratio, curing regime and age. Fig. 2 shows the box-plot representation of 46 results of UHPC/UHPFRCs' water sorptivity at 28 days (data from last column in Supplementary Table S2).

The level of compressive strength at 28 days achieved with each composition, (also included in Supplementary Table S2), ranges from 119 to 213 MPa [13,14,42,55–61].

In fact, same factors as those examined for the porosity also impact the water absorption ability. The binder composition, namely the cement type as well as the presence of either SF or alternative SCM as partial surrogates of cement or SF can impact the water absorption ability [13,14,58,59,61]. Extending the curing time from 28 to 56 or 90 days under normal curing conditions is effective to reduce the sorption coefficient [13,14]. In addition, high curing temperatures also accelerated the hydration reactions, promoting a faster matrix densification regarding the standard curing room and thus, giving rise to lower sorption coefficients. Some studies revealed that steel fibres incorporation to a certain extent decreases the sorptivity [57,60]. This is explained in part by the fibres bridging across the microcracks that are originated due to early ages shrinkage and thus decreasing the pores interconnectivity [57]. The same was not observed in [13] when incorporating 1% of steel fibres to several UHPC mixtures.

Table 1
Classification and limit values for porosity measured by MIP [40].

MIP total porosity (%)	Potential durability
>16	Very low
13–16	Low
9–13	Average
6–9	High
3–6	Very high

Table 2
Quality classification regarding the sorptivity values at 28 days [54].

Sorptivity (kg/(m^2 × h$^{0.5}$))	Concrete quality
>15	Very poor
10–15	Poor
6–10	Good
<6	Very good

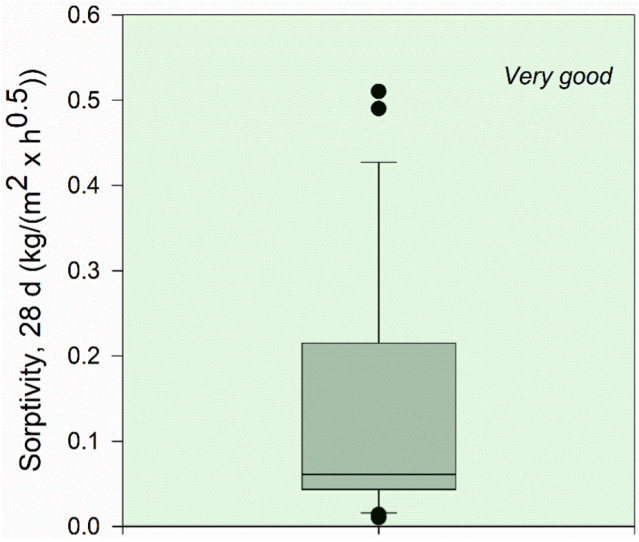

Fig. 2. Box-plot of sorptivity data (28 days) reported in the literature and potential durability classification (as proposed in [54]).

Considering the values represented in Fig. 2, the middle 50 percent of the values fall within the range 0.04 to 0.21 kg/($m^2 \times h^{0.5}$), corresponding to the 25th and 75th percentiles, respectively. A typical value of the sorptivity (the median value) is 0.06 kg/($m^2 \times h^{0.5}$). The water sorptivity values presented in Fig. 2 – markedly smaller than the threshold value for the most demanding class in Table 2 – reveal that UHPCs exhibit a high durability potential for this property. Moreover, according to European standard EN 1504–3 that specifies the performance (including durability) requirements of mortars to be used for the structural and non-structural repair of concrete structures, the sorptivity value, at 28 days, must be equal or lower than 0.5 kg/($m^2 \times h^{0,5}$). Fig. 2 shows that typically UHPCs meet this requirement.

2.3. Resistance to chloride ion penetration

Since chloride ions can trigger and catalyse the reinforcement corrosion, concretes' resistance to chloride ions permeability has been assumed as one of the most important durability indicators. Different test methods have been used for estimating the resistance to chloride ingress on UHPC including both direct tests such as chloride diffusion and migration tests as well as indirect tests based on electrical resistivity or diffusivity [62]. The rapid non-steady-state tests have been more widely accepted than the steady-state tests mainly because the latter tests are very time-consuming. This research adopted the rapid non-steady chloride migration test method (RCM), based on NT BUILD 492. This test uses an external electrical field to accelerate the chloride penetration, providing the non-steady state migration coefficient (D_{nssm}) values (as detailed in section 3.3.3). The D_{nssm} is not directly comparable with chloride diffusion coefficients obtained from the other test methods namely the non-steady-state immersion test and the steady-state migration test. It was established elsewhere [63], a systematic classification of the concretes' resistance to chloride penetration based on the D_{nssm} values. This classification is reproduced in Table 3.

Table 3
Classification and limit values for the D_{nssm} at 28 days [63].

Migration coefficient ($\times 10^{-12}$ m^2/s)	Resistance to chloride penetration
>15	Low
10–15	Moderate
5–10	High
2.5–5	Very high
<2.5	Extremely high

Supplementary Table S3 summarizes 27 results of chloride migration coefficient obtained on UHPC/UHPFRC reported in literature considering binder composition, fibre volume, w/b ratio, curing regime and age. Fig. 3 shows the box-plot representation of 23 values of D_{nssm} at 28 days (data from last column in Supplementary Table S3).

The compressive strength at 28 days achieved with each composition (also included in Supplementary Table S3) ranges from 107 to 172 MPa [61,64-69].

The resistance to chloride-ion penetration is also highly dependent on UHPC composition, namely, nature and proportions of constituents (namely SCM) and w/b ratio [61,64,67], as well as curing regime and curing duration. An air-dried UHPFRC showed significantly higher chloride migration coefficient compared to standard wet-cured UHPFRC, at 28 days [65]. But, the extension of the standard wet-curing from 28 days to 6 months proved to be effective to decrease (by 45%) the chloride migration coefficient [65]. UHPCs exposed to both standard wet-curing and heat-curing (70 °C, for 72 h) showed comparable resistance to chloride penetration [67]. With regard to the influence of fibres, the permeability to chlorides was somewhat higher in UHPFRC [65]. A possible explanation is that when fibres are used in high amounts, bundles can be formed that allow more easily diffusion of chlorides [65].

Considering the values represented in Fig. 3, the middle 50 percent of the values fall within the range 0.38 to 2.35 $\times 10^{-12}$ m^2/s, corresponding to the 25th and 75th percentiles, respectively. The median value is 2.1 $\times$ 10^{-12} m^2/s. Despite the differences in the studies listed in Supplementary Table S3, Fig. 3 shows that the chloride migration coefficients obtained remain within or very close to the range proposed for "Extremely high" durability according to the classification shown on Table 3.

2.4. Resistance to carbonation

In the scope of the cement-based materials, carbonation consists in the formation of calcium carbonate ($CaCO_3$) from the reaction of carbon dioxide (CO_2) with the hydration cement products, CH or CSH. Thus, this process reduces the pH of the cementitious matrices that might promote steel depassivation and also trigger reinforcement corrosion.

Carbonation process depends on diverse variables namely binder composition (type of cement and SCM) and water to cement (w/c) ratio as well as environmental conditions namely concentration of CO_2 and humidity. Independent of the environmental conditions, the resistance to carbonation is mainly determined by the material's porosity and by

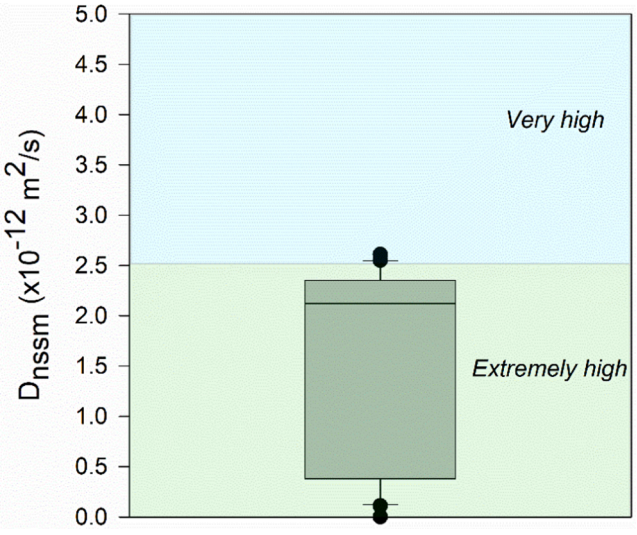

Fig. 3. Box-plot of chloride migration coefficient data (28 days), based on NT BUILD 492 reported in the literature and classification (as proposed in [63]).

the reactivity of the cement phases with CO_2. In UHPC, as discussed before in section 2.1 there is a significant reduction of porosity that hinders the gas permeability decreasing the carbonation rate. However, the use of the high content of SCMs might significantly reduce or even deplete the portlandite content (due to pozzolanic reaction) leading to an increase of the concrete carbonation susceptibility. As such, the feasibility assessment of using a novel high pozzolanic material in the UHPC composition raises the need for evaluating the carbonation risk.

Supplementary Table S4 includes 17 results of resistance to carbonation and compressive strength of UHPC/UHPFRC found in several studies. The resistance of the concretes to the CO_2 penetration is often evaluated by accelerated carbonation test in a CO_2-enriched chamber and with a favourable humidity. Besides the differences in exposure conditions found in [45,47,58,69–74], all studies showed that the carbonation depth on the UHPC/UHPFRC is extremely low.

2.5. Expansive reactions

2.5.1. Alkalis-silica reaction

Alkalis-silica reaction (ASR) in concrete refers to the chemical reaction between alkali cations namely Na^+ and K^+ (present in one of the concrete constituents such as the cement, SCM or admixtures) and a reactive siliceous aggregate. This reaction forms a deleterious expansive product that leads to cracking. According to ASTM C1260 standard, expansion values lower than 0.10%, after 14 days, indicates innocuous behaviour, while values higher than 0.20% suggests a potentially harmful behaviour. The high content of cement, pozzolans and admixtures (as discussed in Section 1) in UHPC mixtures increases the alkali content, and thus its availability to participate on ASR. As such, the assessment of the risk of damage due to this deleterious phenomenon is relevant. Another concern is related to the possible formation of silica fume agglomerates where ASR can be initiated. On the contrary, given the elimination of coarse aggregate and the typical very low permeability of UHPC, some authors [74–76] argue that the occurrence of ASR is improbable regardless the curing regime.

Piérard et al. [74] followed the "Oberholster test" methodology, that consists in a modified ASTM C1260 test procedure to verify ASR susceptibility of an UHPC prepared with w/c = 0.23. In brief, three cylindrical samples (ϕ = 50 mm; l = 160 mm) were hot-cured at 80 °C for 24 h and then their initial length was measured. Then, the samples were immersed in 1 N NaOH solution at 80 °C and their length determined daily for 20 days. No expansion or deterioration were observed after this severe test [74]. Graybeal and Tanesi [75] performed ASR testing on UHPFRC prisms (V_f = 2%, w/b = 0.12) following the ASTM C1260 test procedure. However, to evaluate the occurrence of additional curing of the UHPC matrix due to the hot curing at 80 °C, prescribed in the ASTM C1260 test procedure, two additional sample sets were tested using different curing regimes: one set remained at ambient laboratory conditions during 28 days before starting the ASR testing, whereas on the other set the ASR testing began as soon as the samples were demoulded. The expansion results obtained on all UHPC were one order of magnitude below the lower limit threshold of 0.1% both after 14 and 28 days of testing [75]. Soliman and Tagnit- Hamou [77] followed the standard ASTM C 1260 testing procedure to evaluate the ASR expansion of UHPC prepared with 0, 50, and 100% of glass sand. The UHPC samples showed a maximum expansion of 0.03% at 16 days, that is remarkably lower than the limit of 0.1% specified in the standard. Sawab et al. [78] tested some UHPC mixes containing quartz sand, following ASTM C1260 procedure. The UHPC specimens showed negligible expansion up to 14 days. Moser et al. [76] used a cyclic climate storage to simulate the climate conditions in Central Europe in an accelerated manner, and found that UHPC specimens showed an expansion value below the threshold limit of 0.04% after 603 days, regardless the curing regime (water storage or heat-treated).

In summary, a general conclusion from these studies is that ASR is not a concern for UHPC/UHPFRC under any curing regime due to the low permeability.

2.5.2. External sulphates

Ingress of external sulphates can promote length change in cement-based materials in the hardened-state, associated to the formation of expansive calcium sulfoaluminate hydrates. However, due to the very low permeability of UHPFRC as well as the low content of CH consumed in the pozzolanic reactions, the risk of external sulphate attack is generally considered minimal, and for this reason limited research on this topic has been performed.

Ahmad et al. [79] prepared an UHPFRC with 2.0% steel fibres and w/b = 0.15. The authors tested the resistance to sulphate attack on 50 mm cubic samples after 28 days of water curing followed by their immersion in a sulphate solution (2.5% $MgSO_4$ and 2.5% Na_2SO_4) for 6 months. The sulphate attack was assessed based on compressive strength decrease. The very low compressive strength loss (7%) observed on the UHPFRC exposed to those severe sulphate conditions confirmed its high resistance against sulphate attack [79]. The resistance to sulphate attack of several RPC was tested according to ASTM C 1012 by Chuang and Huang [80]. After 28 days of water curing, the initial length of the 75 × 75 × 285 mm^3 samples was determined and, then, the specimens were immersed in the Na_2SO_4 solution for 12 months. The evaluation of the specimens' length revealed that the UHPCs expansion (<0.01%) was much lower when compared with ordinary concrete with w/b = 0.48 (~0.05%). Moreover, UHPFRC with higher water to binder ratio (from w/b = 0.25 to w/b = 0.30) and without fibres exhibited higher expansion, as it would be expected [80]. Piérard et al. [81] evaluated the sulphate resistance of three different mixtures of UHPC, including different type of binder, aggregate and w/c (0.30 and 0.23). The test was based on CUR Recommendation 48. The UHPC prisms (40 × 40 × 160 mm^3) tested were immersed in a sodium sulphate solution, and the dimensional change was determined periodically. The results showed neither length variation nor deterioration even in the mixtures that were immersed for 500 days [81]. El-Dieb [82] exposed UHPFRC with different twisted-steel fibre contents (0.08%, 0.12% and 0.52%) to a high concentration sulphate solution (5% sodium sulphate, by mass) and under high temperature (50 °C), resembling the Gulf environment. The compressive strength of the UHPFRC was determined at different time intervals after immersion in the sulphate solution (up to 12 months) and compared with the compressive strength obtained at 28 days. The authors reported a compressive strength decrease of about 12%, even in the samples immersed in that high concentrated sulphate solution for 12 months. Moreover, the incorporation of fibres showed no significant effect on the resistance to the high sulphate and high temperature exposure conditions [82].

These studies confirm the very low permeability of UHPC keeps sulphate ions out of the UHPC/UHPFRC, significantly reducing the risk of degradation from external sulphate attack.

2.6. Final remarks

The data collected in the literature survey seem to be appropriate for a valid and useful systematic assessment of the mixture parameters and their effect on the durability properties in terms of statistical expression. Most importantly, these data are useful for benchmarking purpose regarding the UHPC containing ECat employed in the current investigation and which durability assessment results are presented in Section 4.

3. Materials and methods

3.1. UHPC mix design

The non-proprietary UHPC employed in this study was optimised by the authors in a previous study [34]. UHPC mix-design was carried out using a statistical factorial design approach, namely a central composite

design, followed by a numerical optimization technique to ensure its self-compacting ability, high compressive strength and electrical resistivity at 28 days as well as low autogenous shrinkage at early ages.

Raw materials consisted of ordinary Portland cement (Type CEM I and strength class 42.5 R, according to European standard EN 197–1), silica fume ($SiO_2 > 90\%$), limestone filler (98% $CaCO_3$), siliceous natural sand, ECat (the by-product originated in the fluid catalytic cracking unit of the Sines Refinery in Portugal), potable water and a high-range water reducer polycarboxylate-based superplasticiser (Sp), Viscocrete 20HE, supplied by Sika. Table 4 shows the chemical composition of the ECat obtained by X-ray fluorescence spectrometry (XRF) and the loss on ignition (LOI) evaluated following EN 196-2. Table 5 shows the main physical properties of all solid materials (detailed in [34]).

Table 6 presents the proportions of UHPC mixture under study, corresponding to an effective w/b ratio equal to 0.17 and an effective w/c ratio equal to 0.23. In this mixture, the aggregate fraction consisted of 85% siliceous natural sand and 15% ECat, by volume. Since ECat has a high specific surface area (Table 5) with water affinity can absorb a significant amount of water (30%, by mass). Thus, this UHPC used ECat as an internal curing agent with beneficial effect to reduce its autogenous shrinkage, as shown in the previous investigation [34].

In the previous investigation, the UHPC mixture presented in Table 6 was also prepared with 3% high-strength steel fibres ($l_f = 13$ mm; $d_f = 0.2$ mm) and revealed good deformability in the fresh state (average slump flow diameter of 282.5 mm, without compaction energy) and compressive strength of 147 and 156 MPa at 28 and 90 days, of wet curing at 20 °C, respectively. A mixture revealed a strain-hardening behaviour in tension leading to multiple microcracking formation (uniaxial tensile peak stress and peak strain ranging from 11 to 15 MPa and 0.27–0.47%, respectively, at 28 days). Further details concerning the origin and characteristics of ECat, the mixture design approach, as well as the properties of this nonproprietary mixture), can be found elsewhere [34].

3.2. Mixing procedure and samples preparation

The UHPC was prepared using a mortar mixer with a vertical axis (in accordance with standard EN 196–1) at a low speed of 140 rot/min. The mixing sequence was as follows, except for preparation of MIP testing samples in which the difference is that the sand was not added:

- adding ECat (dry state) with 80% of mixing water plus the water required for the ECat saturation and mixing for 5 min
- adding sand, cement, SF, LF and mixing for 2.5 min
- stopping the blender to scrape material adhering to the mixing bowl and mixing for more 2.5 min
- adding the remaining the water with 75% of Sp, and mixing for 2.5 min.
- adding the remaining Sp and mixing for 3.5 min.

It should be noted that the incorporation of ECat leads to an increase in the duration of mixing, in the initial part, to allow the ECat saturation with water. After mixing, the moulds were filled at once without mechanical vibration since the mixture is self-compacting. Then, samples were covered with a plastic sheet and demoulded after 1 day.

Different moulds (shape and size) were used to prepare the test samples, depending on the durability property to be evaluated, as shown in Table 7. Samples were cured in a chamber at 20 ± 2 °C and HR > 95%, until the age of testing, excluding the samples for carbonation and expansive reactions tests which followed specific curing regimes (sections 3.3.4, 3.3.5 and 3.3.6).

3.3. Scanning electron microscopy

Cross-sections surfaces of UHPC pastes (without sand) at 28 and 90 days of hydration were imaged using High resolution (Schottky) Environmental Scanning Electron Microscopy (SEM) using back-scattered electron (BSE) mode couple with Energy Dispersive X-ray Spectroscopy (EDS), FEI Quanta 400 FEG ESEM / EDAX Genesis X4M.

The interruption of the hydration reactions on the UHPC samples followed the procedure that is currently considered the most suitable for further microstructural analysis of hardened cement–based materials [50,83,84], which consists of solvent replacement with isopropanol followed by drying. As such, the UHPC sample was immersed in a 99.8% isopropanol solution for 7 days, followed by drying in an oven at 40 °C for 48 h, and then further dried in a vacuum chamber for 24 h. The hardened UHPC samples were impregnated in a low viscosity epoxy resin and subsequently polished incrementally until a flat surface was achieved. The polished samples were sputter-coated with a Au/Pd thin film just prior to SEM examination. The images were obtained at an acceleration voltage of 15 kV and at a working distance of 10 mm.

3.4. Test methods

Diverse durability indicators were assessed on the hardened state of the newly developed UHPC mixture with ECat incorporation to allow for a direct comparison with results from UHPC mixtures reported in literature (summarised in Section 2), as well as, to evaluate how far this class of material is superior to that of normal- and high-strength concretes.

Table 7 lists the selected durability tests which are further described in the following sections. When applicable, the test procedures were based on international standards and/or specific Portuguese recommendations.

3.4.1. Mercury intrusion porosimetry

The total porosity and pore size distribution were determined at 28 and 90 days by MIP using an Autopore IV 9500 instrument (Micromeritics), which can measure pore sizes from 400 μm to 0.004 μm. This test used the contact angle of 140°, surface tension of 485 mN/m, and applied low and high pressures of 0.5 and 3300 psi, respectively. Prior the testing, the hydration reactions were interrupted at 28 and 90 days by immersing the samples during 7 days in 99.8% isopropyl alcohol, drying at 40 °C in an oven for 48 h and then vacuum drying for 24 h.

3.4.2. Water absorption by capillarity

The water absorption by capillarity was determined on five replicates of UHPC prismatic samples (Table 7), following the recommendation RILEM TC 116-PCD. In brief, the procedure consisted of drying the samples in a ventilated oven at 40 °C until reach constant mass. Then, the test samples were placed in a water bath which level was automatically adjusted so that the face of the sample was kept immersed to a constant depth of approximately 3 mm. The mass of the samples was evaluated at time intervals after contact with water (5, 10, 20, 30, 60, 90, 120, 180 and 240 min) up to four hours from its first contact with water. The samples were kept at temperature of 20 ± 2 °C and HR higher than c.a. 50%.

Table 4
Bulk chemical composition of ECat obtained by XRF.

	Chemical composition (% by mass)												
	SiO_2	Al_2O_3	Fe_2O_3	CaO	MgO	K_2O	Na_2O	TiO_2	P_2O_5	V_2O_5	NiO	La_2O_3	LOI
ECat	40.30	54.45	0.45	0.06	0.15	0.02	0.43	0.72	0.50	0.33	0.42	0.87	1.05

Table 5
Main physical properties of constituent materials.

	Cement	LF	SF	ECat	Sand
Specific gravity (kg/m^3)	3110	2668	2200	2660	2570
Specific surface area (m^2/kg) (*Determination method*)	438 (*Blaine*)	540 (*Blaine*)	19,632 (*BET*)	150,070 (*BET*)	–
Size distribution (*Determination method*)	(*Laser diffraction*)	(*Laser diffraction*)	(*Transmission Electron Microscopy*)	(*Laser diffraction*)	(*Sieving*)
d_{10} (μm)	1.4	0.7	0.11	59	100
d_{50} (μm)	20	3.2	0.13	79	320
d_{90} (μm)	25	10	0.80	140	520
24 h water absorption (%) (*EN 1097–6*)	–	–	–	30	0.5

Table 6
UHPC mixture proportions.

	Raw Materials	(kg/m^3)
Binder phase	Cement	690.19
	Silica fume	33.56
	Limestone filler	250.58
Aggregates	ECat	155.45
	Siliceous sand	852.11
Admixture	Superplasticizer	19.49
Water	Total*	207.50
(*) of which 46.64 kg/m^3 corresponds to ECat's absorbed water		

The water intake per unit area (i) was determined, over time, dividing the mass of water absorbed (kg) by the cross-sectional area of the test face exposed to water (m^2). The sorptivity, S (kg/(m^2 × h$^{0.5}$)), of each replica sample, consisted in the slope of the graph of the water intake per unit area (kg/m^2) versus the square root of the immersion time (h$^{0.5}$). The corresponding average was taken as the sorptivity for the UHPC under study.

3.4.3. Rapid chloride migration test

The resistance to chloride migration was evaluated, at both 28 and 90 days, on six replicates of UHPC cylindrical samples (Table 7), according to the procedure set out in the standard NT Build 492. Briefly, the samples were vacuum soaked with a $Ca(OH)_2$ saturated solution. Afterwards, it was applied an electrical potential across the samples to force the chloride ions present in the catholyte solution (10% NaCl) to migrate through them. Based on the initial electrical current measured, the voltage and the test duration were adjusted (6 to 96 h) in compliance with the values set out in the standard NT Build 492. The samples were then axially break into two halves, and the surfaces freshly splitted were sprayed with a silver nitrate solution (0.1 M) leading to the precipitation of the insoluble white silver chloride salt. The chloride penetration depth corresponded to the precipitated salt depth (Fig. 8). The non-steady-state migration coefficient, D_{nssm}, was calculated using Equation (1) for each sample replicate, and the average is considered the D_{nssm} for UHPC under study.

$$D_{nssm} = \frac{0.0239(273+T)L}{(U-2)t} \times \left(x_d - 0.0238\sqrt{\frac{(273+T)Lx_d}{U-2}} \right) \times 10^{-12} \quad (1)$$

where U is the absolute value of the voltage applied (V); T is the mean value of the initial and final temperatures in the 0.3 M NaOH anolyte solution (K); x_d is the mean value of the penetration depths (mm), L is the sample thickness (mm); and t is the duration of the test (h).

To complement the testing, the chlorides content at different depths was evaluated in one half of one of the samples tested at 28 days (in concrete in the one that adopted the reference B-2.1 in Table 8). The powdered samples were sampled using the "dry drilling method" described in the RILEM Recommendation TC 178-TMC in incremental depth steps of approximately 5 mm. Three samples for analysis were collected, at to 0–5 mm, 5–10 mm and 10–15 mm depths. Determination

Table 8
Rapid chloride migration test results obtained in replicates samples of the UHPC, at 28 and 90 days of curing.

Curing time	Sample reference	t (h)	U (V)	Average temperature during test (°C)	X_d (mm)	D_{nssm} (×10^{-12} m^2/s)
28 days	B-1.1	24	40	22.1	5.68	1.77
	B-1.2			21.5	6.43	2.03
	B-1.3			21.8	6.07	1.91
	B-2.1			22.0	6.39	1.99
	B-2.2			21.7	6.78	2.12
	B-2.3			21.9	6.60	2.09
90 days	A-1.1	96	60	22.6	6.58	0.36
	A-1.2			22.3	7.28	0.39
	A-1.3			21.9	7.60	0.41
	A-2.1			22.7	7.23	0.39
	A-2.2			22.2	6.44	0.34
	A-2.3			22.2	5.52	0.29

Table 7
Durability testing plan carried out the on UHPC mixture with ECat incorporation.

Durability indicator	Test standard	Testing age	Number of samples for each age	Samples geometry and size
Total porosity and pore size distribution	(*No test standard applicable*) Technique used: MIP	28, 90 days	1	Cylindrical h = 25 mm, Ø=8 mm
Water absorption by capillarity	RILEM TC 116-PCD	28 days (+14 days at 40 °C, until constant mass)	5	Prismatic 40 × 40 × 45 mm^3
Resistance to chlorides migration	NT Build 492	28, 90 days	6	Cylindrical h = 50 mm, Ø=100 mm
Carbonation resistance	RILEM CPC-18	3, 6, 9 and 12 months	3	Prismatic 40 × 40 × 160 mm^3
Risk of alkali-silica reaction	ASTM C 1260 (set 1, Fig. 3)	up to 184 days	3	Prismatic 25 × 25 × 250 mm^3
	ASTM C 1260 adapted (set 2, Fig. 3)	up to 184 days	3	
Resistance to sulphate attack	Portuguese specification LNEC E-462	up to 26 weeks	6	Prismatic 20 × 20 × 160 mm^3

of chloride content was performed by chemical analysis according to standard NP EN 196–2.

3.4.4. Accelerated carbonation test

The resistance to carbonation was evaluated at 3, 6, 9 and 12 months, on three replicates of UHPC prismatic samples (Table 7) following the procedure described in the RILEM CPC-18. The samples were wet cured for 14 days, and then placed in a room with controlled temperature and RH (20 ± 2 °C and 50 ± 3%, respectively) for 14 days. Thereafter, the samples were kept in an accelerated carbonation chamber of 5 ± 0.1% CO_2, RH of 60 ± 5%, and temperature of 23 ± 2 °C. At testing ages, a slice with approximately 1 cm thickness was cut from each sample, and the freshly splitted surfaces were sprayed with 1% solution of phenolphthalein. Since the phenolphthalein turns pink on non-carbonated areas the carbonation area was assessed by the depth of the sample area in which the phenolphthalein remains colourless.

3.4.5. Expansion due to ASR

The risk of occurrence of alkali-silica reaction in UHPC was monitored following the test procedure prescribed in the American standard ASTM C 1260 with three modifications. The first modification was the materials and mix-proportions used. Instead of using the mortars proportioning specified in the standard, the samples were produced to replicate the non-proprietary UHPC under study, using the materials and mix-proportions indicated, previously, in section 3.1.

Another modification was the curing method. The procedure described in the standard ASTM C 1260 specifies the samples demoulding after 24 h, subsequent placement in an 80 °C water bath for 24 h, and then their placement in an 80 °C sodium hydroxide solution bath until test conclusion. The samples submerging in a water bath at 80 °C is fairly equivalent to the steam-based curing regimes consisting in placing the samples in a high-heat, high-humidity environment. Hence, it was anticipated that the test method described in standard ASTM C 1260 may lead to an unintentional hydration acceleration of the UHPC regarding the normal curing that was intended to the mixture with ECat under study. Thus, two sample sets were prepared for testing. Samples of Set 1 were cured following the ASTM C 1260 procedure whereas the samples of Set 2, undergone 28 days curing at 20 °C and HR > 95% before immersing in an 80 °C sodium hydroxide solution bath. Fig. 4 presents schemes of the two curing regimes.

Three prismatic samples (Table 7) were cast for each set, and the average is considered the expansion due to ASR. The initial reading (L_0) for the samples of Set 2 was measured at 28 days instead of their length after 24 h immersion in hot water as it is prescribed in the standard and followed for samples of Set 1 (Fig. 4). After the initial reading, the length changes were monitored periodically (about 3 times per week, during the first 2 weeks, and then once a week) up to 28 days of immersion in NaOH solution. Afterwards, the assessment of length change was performed every two weeks and the test was concluded when samples achieved an ASR expansion approximately of 0.1% (after half a year in NaOH solution, as it will be presented in section 4.5).

3.4.6. Expansion due to external sulphates

The resistance to external sulphate attack of the UHPC was evaluated on six replicates of UHPC prismatic samples (Table 7) following the procedure described in the Portuguese LNEC specification E-462. The samples remained in the mould 24 h after casting and then were demoulded and immersed in saturated calcium hydroxide ($Ca(OH)_2$) solution at 20 °C, during 28 days. At that time, the length of the samples was measured for reference as the initial reading (L_0). Thereafter, two curing conditions were adopted i.e., half of the samples were immersed in a sodium sulphate solution (16 g/l SO_4^{2-}) (that was renewed every 2 weeks) and the remaining samples were maintained in the $Ca(OH)_2$ saturated solution. The samples length was monitored throughout 168 days every two weeks. The expansion due to external sulphates is the difference between average expansion of sulphate cured samples and the $Ca(OH)_2$ cured samples.

4. Results and discussion

4.1. SEM/EDS microstructure characterization

Fig. 5 shows BSE-SEM images of the microstructure of the UHPC paste at 28 and 90 days of hydration as well as corresponding EDS spectra of local chemical analysis performed on selected regions. The BSE-SEM images revealed the homogenous spatial distribution of the solid phases, including the ECat particles (regions A), in the cementitious matrix as well as that the ECat particles reserve their original shape and size over the hydration time. Moreover, the EDS spectra obtained on the ECat particles (regions A) confirmed their pozzolanic nature (ability to react with portlandite) associated to the progressive diffusion of calcium into the particles.

The contrast of the polished flat-surfaces BSE-SEM images arises mainly from the differences in the chemical composition of the phases present [84]. Thus, the polymineral cement particles are identified in the BSE-SEM analysis (for example, regions B in Fig. 5) by the various

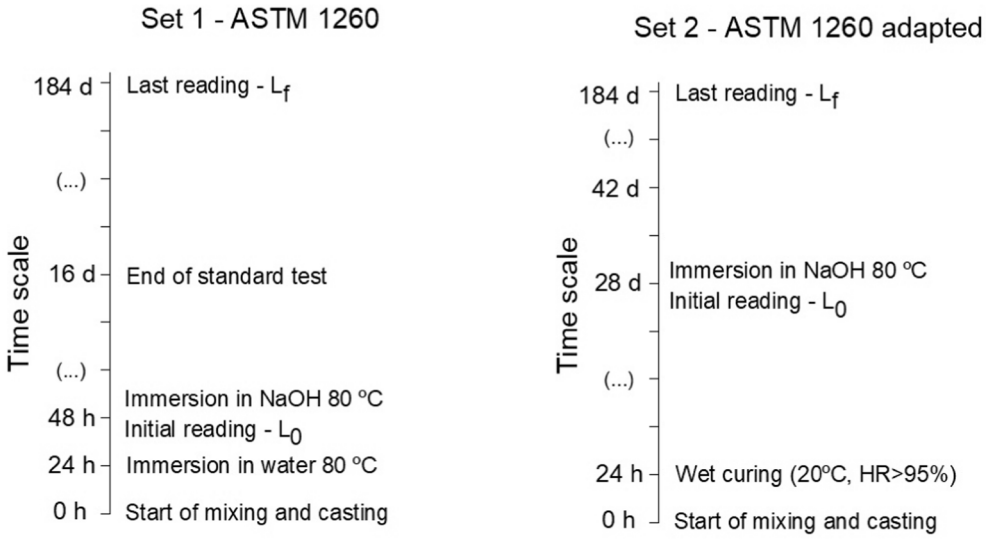

Fig. 4. Curing methods of samples sets for ASR testing: a) Set 1 – following standard test; b) Set 2 - adapted curing method.

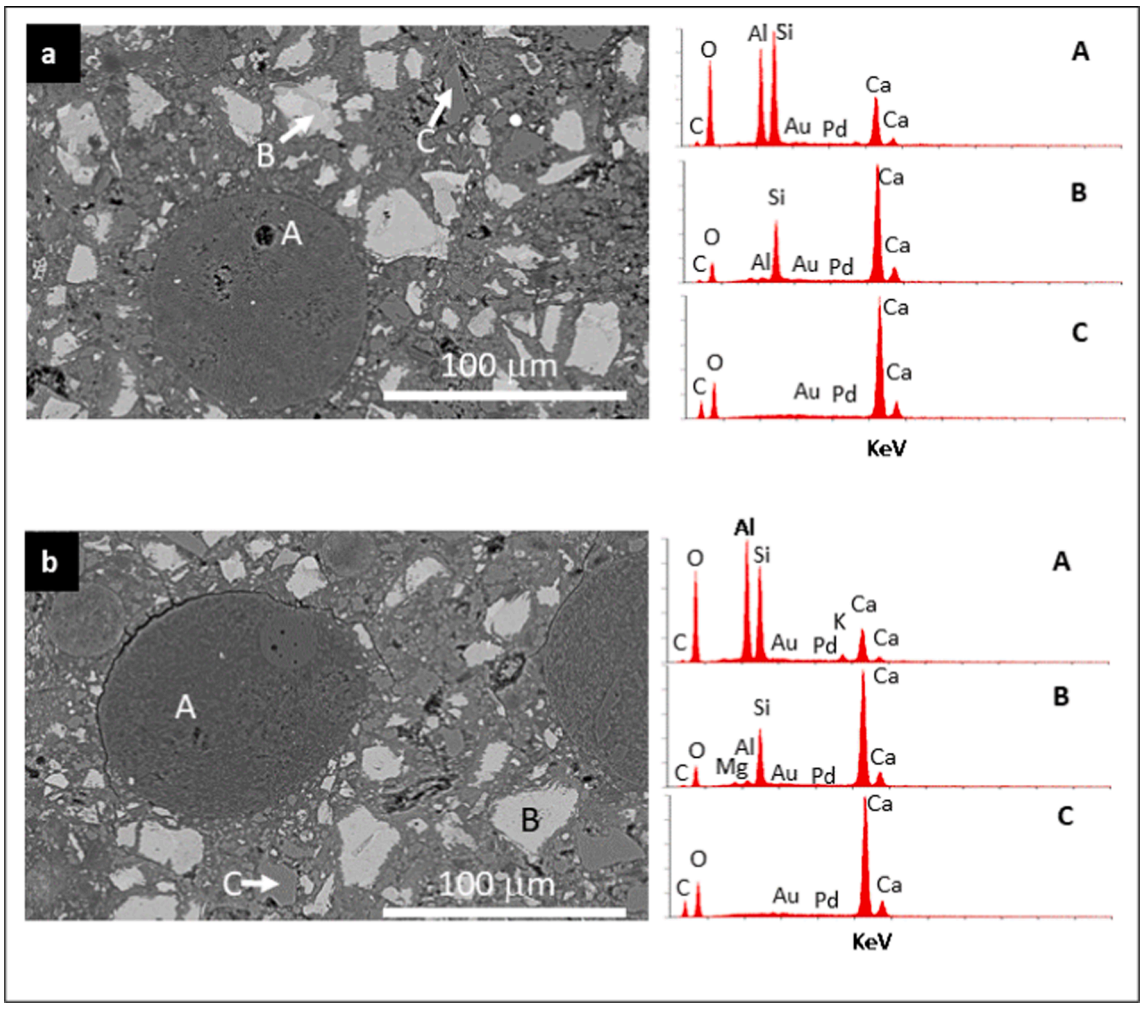

Fig. 5. BSE-SEM images of cross-sections surfaces of the UHPC paste at (a) 28 days and at (b) 90 days of hydration and corresponding EDS spectra of local chemical analysis performed on selected regions: A – ECat particle, B – cement particle, C – limestone particle.

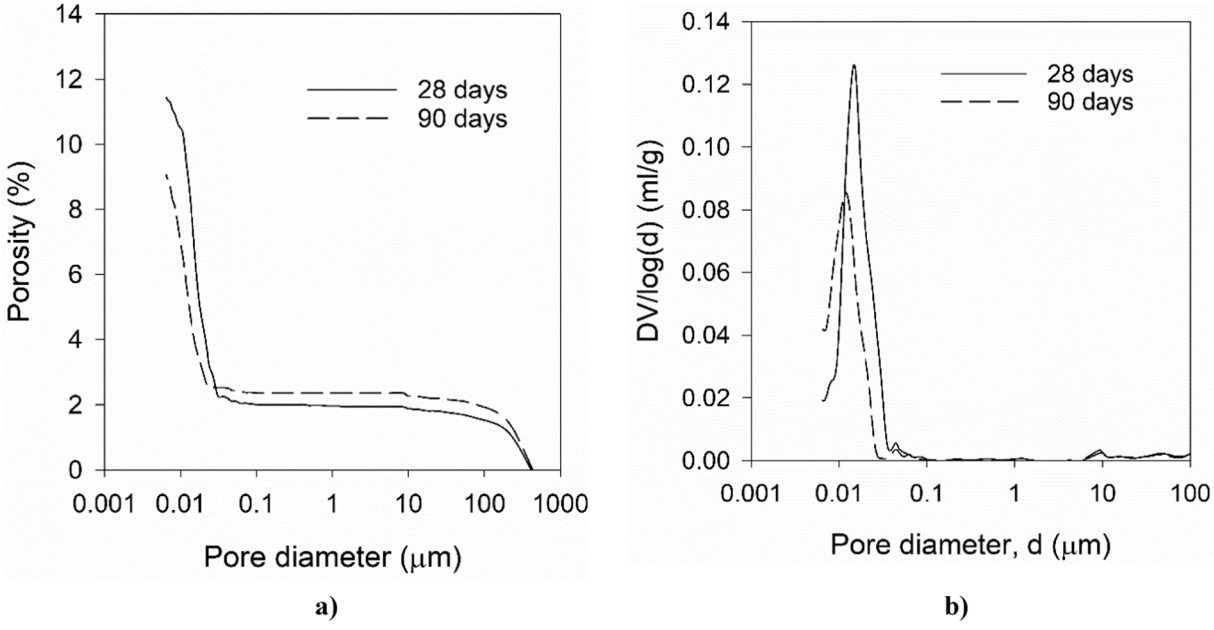

Fig. 6. Pore structure of UHPC at 28 and 90 days: (a) cumulative porosity and (b) differential pore size distribution.

grey levels that their images exhibit while the images of the limestone particles present a homogeneous grey tone (for example, regions C in Fig. 5). In addition, BSE-SEM analysis showed that at 90 days of hydration, the inner core of the cement particles remains unhydrated exhibiting higher contrast (associated to its higher electron density) in the images than the layer of the hydrated compounds that forms over time in the cement particles boundary.

At 28 days of hydration, the BSE-SEM images already showed reduced content of distinctly visible (black) pores indicating that either the sample present low total porosity or that the pores are too small to be resolved by this technique. At the usual range of magnifications, qualitative BSE-SEM analysis typically do not resolve pores lower than about 0.2 μm [85]. Thus, the porosity assessment of the cementitious materials with low w/c ratio like that under study requires either the application of image processing techniques [86] or the use of other experimental technique such as MIP (section 4.2).

4.2. Mercury intrusion porosity

Fig. 6 shows the MIP pore size distribution of the UHPC at 28 and 90 days. The UHPC total porosity, at 28 days, was 9.94%, which is slightly above the upper quartile of the results found in the literature, shown in box-plot of Fig. 1. However, a deeper analysis of the porosity results reveals that it is mostly, namely 9.43%, in the range of gel pores (4–100 nm pore diameter) while only to the remaining 0.51% lies in the range of the capillary porosity (100–80 000 nm) which are the more critical in terms of durability assessment. Moreover, with the progress of hydration reactions, from 28 to 90 days, the total porosity decreased to 7.15% (of which 6.70% is gel porosity and 0.45% is capillary porosity). The critical pore diameter that corresponds to the first peak of the differential curve (Fig. 6(b)) reduced from 15.3 to 11.9 nm, and the magnitude of the peak decreased.

According to the classification proposed in Table 1 [40], the total porosity of 9.94%, at 28 days, of the new UHPC with ECat incorporation (under study) lies in the boundary of the region where materials are considered to have of “Average”/”High” potential durability. But at 90 days (total porosity, 7.15%) its classification it is already undoubtedly of “High” potential durability regarding this property.

Moreover, although the literature survey revealed that concerning the total porosity obtained on UHPC at 28 days, the 25th and 75th percentiles range of results lies in the region 4–8% (Fig. 1), several studies already reported values above that found for the UHPC with ECat incorporation under study. In fact, the highest value of 18% was obtained on a UHPC which binder comprised CEM I 42.5, silica fume and 6.4% nano-$CaCO_3$ cured under lime saturated water at 20 °C (Supplementary Table S1).

4.3. Water absorption by capillarity

Fig. 7 plots the cumulative capillary water absorbed (mass change per unit of inflow area) obtained for replicate samples of the UHPC with ECat incorporation, at 28 days of age, versus the square-root of elapsed time of immersion in water during the first 4 h of measurement. The average sorptivity is $0.111 \pm 0.006 \times kg/(m^2\ h^{0.5})$. The result obtained is within the 25th and 75th percentiles range of box-plot in Fig. 2.

Binary and ternary binder blends ready-mixed concretes comprising fly-ash and ECat (generated by the Portuguese oil refinery) presented sorptivity results above $0.3\ kg/(m^2 \times h^{-0.5})$ [33]. Thus, the UHPC understudy presented a much lower sorptivity that may be due to its very low water content, the presence of pozzolanic materials (SF and ECat) as well as the lack of coarse aggregates that contribute to cementitious matrix densification associated to a remarkably lower and discontinuous capillary porosity that reduces the capillary absorption ability. Moreover, these results are in accordance with the new UHPC low porosity revealed by MIP (section 4.1).

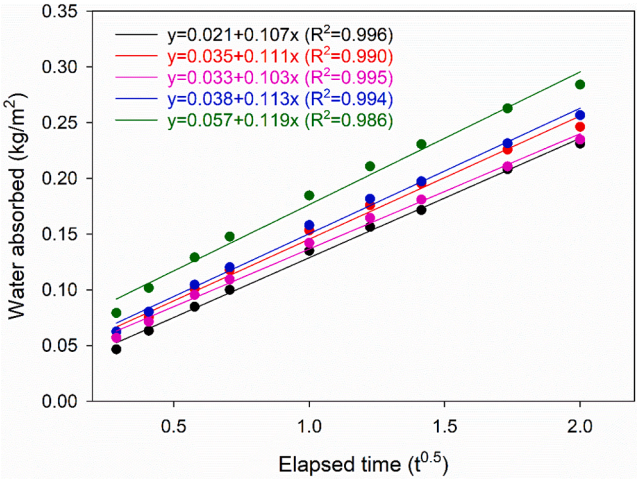

Fig. 7. Experimental results, and corresponding linear regression, of water absorption by capillarity during the first 4 h of contact with water obtained on five replicate samples of the UHPC with ECat incorporation.

4.4. Chloride ion penetration

Table 8 shows the chloride penetration depths (X_d), obtained for replicate samples of the new UHPC at 28 and 90 curing days, as well as, the corresponding non-steady state chloride migration coefficients, D_{nssm}. The average values of D_{nssm} are $2.0 \pm 0.1 \times 10^{-12}$ and $0.36 \pm 0.04\ m/s^2$ at 28 and 90 days, respectively. These results are of the same order of magnitude of those found in the studies for UHPC/UHPFRC reported in the literature (Section 2.3). In particular, the D_{nssm} value at 28 days lies in the 25th and 75th percentiles range of the boxplot of Fig. 3 thus classified as extremely high resistent towards chloride penetration (Table 3).

For ready-mixed ordinary concretes incorporating the same ECat as that used in this study the D_{nssm}, at 28d of age, is $17 \times 10^{-12}\ m^2/s$ [33]. Thus, the UHPC under study is expected to be more resistant in terms of chloride attack. In fact, the ingress behaviour of chloride ions in the cement-based composite matrix is affected by several factors which are partly related both to the characteristics of the cement composite material and to the composition of the external salt solution [87]. In fact, depending on the solution ionic concentration, the chloride ions can only penetrate capillary pores above a certain size [87]. Thus, if the capillaries or the pore sizes become small enough, it is less likely for the ions to be able to diffuse into the cementitious matrix, even at a high solutions concentration [87]. As identified by MIP results, the volume of capillaries pores in UHPC is low and the capillary network is hardly connected (in accordance with sorptivity results) which significantly increases the resistance to the chlorides entrance.

In addition, the small penetration depth identified by the colourimetric analysis, Fig. 8, seems to be in accordance with chloride content determination by the chemical analysis presented in Table 9. Significantly higher content of chloride was found between 0 and 5 mm, but it drastically reduces as it is further from the penetration front.

4.5. Carbonation depth

Although the accelerated carbonation test was carried out for up to 12 months, which is considerably long since this test typically last <3 months, no carbonation could be detected on the tested UHPC, as shown in Fig. 9. The literature review presented in Section 2.4 corroborated the findings of the present study.

4.6. Expansion due to ASR

Fig. 10 presents the expansion results of the UHPC with ECat

Fig. 8. Split surfaces of cylinder samples after the rapid chloride permeability test at 28 days; chlorides ingress from the side of the bottom surface (penetration depth of chloride ions in the lighter part).

Table 9
Chloride content on B-2.1 UHPC sample, tested at 28 days.

Penetration depth from chloride front	Chloride content by mass of sample
0–5 mm	0.470%
5–10 mm	0.240%
10–15 mm	0.056%

incorporation obtained on the ASR test. As already referred, according to standard ASTM C 1260, values of mortar expansion lower than 0.10% at 14 days of testing indicate innocuous behaviour. Since in this case, the expansion after 14 days of testing for samples of Set 1 (according to standard curing method) was of 0.018 ± 0.002% i.e., one order of magnitude below the threshold referred in the standard it is indicative that no deleterious expansion due to ASR is anticipated in the UHPC in most cases. Although after 28 days of water curing, samples of Set 2, exhibited an expansion slightly higher, namely 0.072 ± 0.002%, it was still lower than the reference threshold value of 0.1%. Even after long exposure to NaOH solution, for 184 days, samples also showed no visual evidence of significant deterioration (Fig. 11 and Fig. 12).

These results revealed that ASR expansion of the newly UHPC understudy represent no concern. This behaviour is in accordance with previous findings obtained in other UHPC/UHPFRC, as reported in section 2.5.1. Moreover, the occurrence of alkali-silica reaction requires the presence of water, and since the UHPC under study exhibited low open porosity including to water (Section 4.1) this deleterious reaction is disfavoured. In addition, the ECat possesses a three-dimensional network microstructure with a very high specific surface area (15,0070 m^2/kg, Table 5) with adsorption affinity for cations. As such, the ECat has alkali-ions trapping ability that leads to a reduction of these

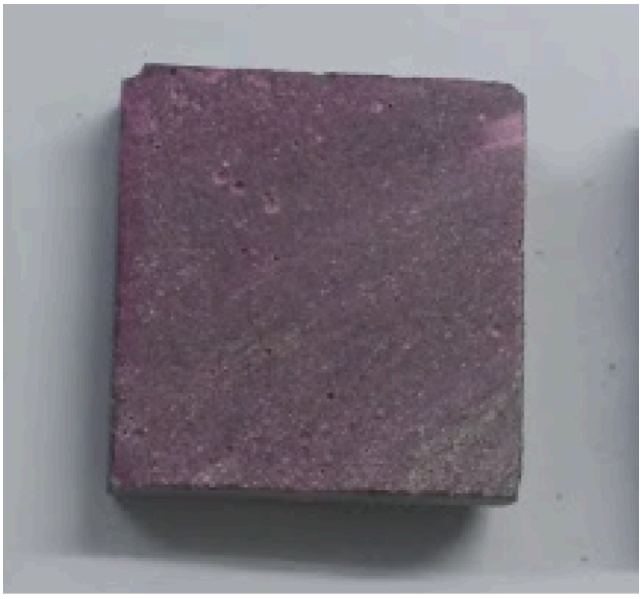

Fig. 9. Freshly split surface of a UHPC sample with ECat incorporation sprayed with the phenolphthalein solution after spent 12 months in an accelerated carbonation chamber (pink surface indicates no-carbonation occurrence). (For interpretation of the references to colour in this figure legend, the reader is referred to the web version of this article.)

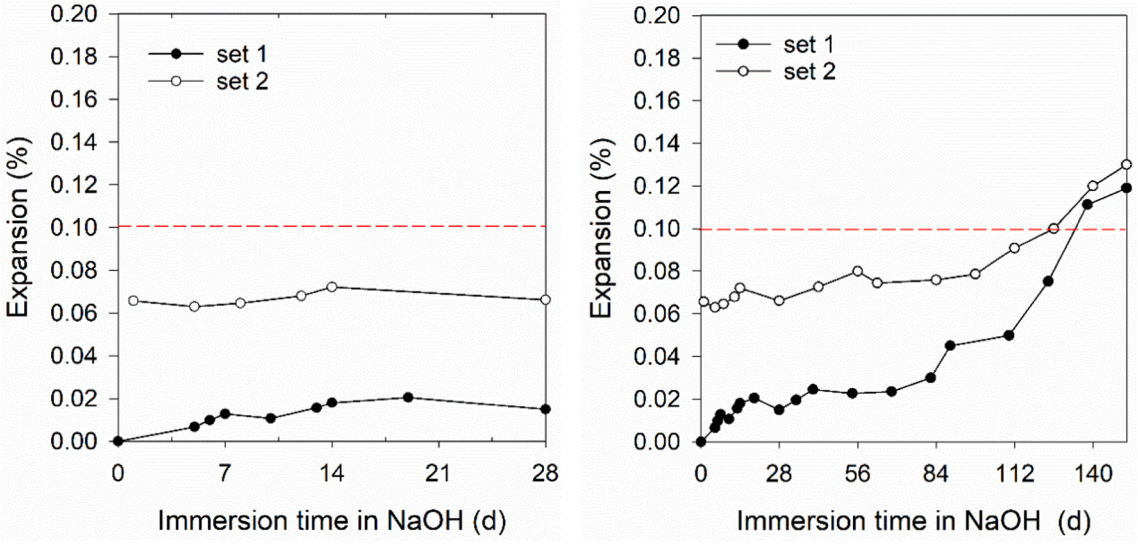

Fig. 10. Change in length of UHPC bar samples used in the ASR testing (Notes: figure a) is a magnification of figure b) focusing on the first 28 curing days; Set 1 – standard curing method; Set 2 – non-standard curing method).

Fig. 11. UHPC samples (Set 1) after long term ASR test.

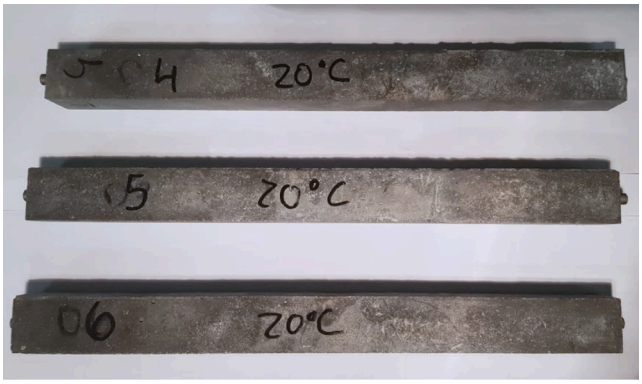

Fig. 12. UHPC samples (Set 2) after long term ASR test.

ions availability to react with the siliceous aggregates. In fact, a previous study [37] on mortars using the same ECat in the binder composition as well as reactive sand showed that the increased content of ECat up to 15% (w/w) significantly mitigates the ASR expansion up to 46% concerning the mortar without ECat incorporation.

4.7. Expansion due to external sulphates

In terms of expansion due to external sulphates attack, UHPC showed superior performance, without dimensional variations up to 26 weeks of exposure to rich sulphate solution. These results are corroborated with no deterioration of UHPC samples verified in their visual examination (Fig. 13). These findings are supported with previous studies performed on other UHPC/UHPFRC, found in literature and already discussed in section 2.5.2.

4.8. Summary of test results

To sum up, Table 10 presents the average and standard deviation of test results, for each durability property investigated under this study, as well as the correponding potential durability in accordance to Tables 1 to 3 and susceptivity to carbonation and expansive reactions.

The experimental results in Table 10 extrapolate the evidence of ultra-high performance of the new UHPC beyond its low early age shrinkage, self–compacting ability and mechanical strength (showed in a previous study [34]) to include its durability. Moreover, the review on other commercial and non-proprietary UHPC/UHPFRC investigations

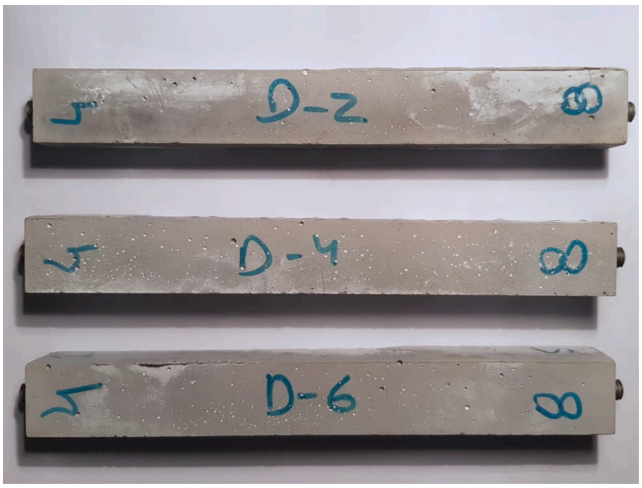

Fig. 13. UHPC samples after 168 days of sulphate solution exposure.

Table 10
Summary of the durability test results for new UHPC and corresponding durability/risk potential.

Durability property indicator	Average ± standard deviation	Potential durability/risk of occurrence
Porosity (MIP) (%)	9.94 (28 d) 7.15 (90 d)	Average
Sorptivity (kg/($m^2 \times h^{0.5}$))	0.111 ± 0.006 (28 d)	Very Good
D_{nssm} ($\times 10^{-12}$ m^2/s)	2.01 ± 0.10 (28 d) 0.36 ± 0.04 (90 d)	Extremely high
Carbonation depth (mm)	0 (after 1 year of exposure)	No risk
ASR expansion (%)		No risk
- ASTM C 1260 (set 1)	0.018 ± 0.002 (28 d)	
- ASTM C 1260 adapted (set 2)	0.072 ± 0.002 (28 d)	
Sulphate expansion (%)	0 (168 d)	No risk

(Section 2) also showed that, in general, the results obtained in the current study are well comparable with the results found in literature survey obtained under similar curing conditions and using the same experimental procedures.

5. Conclusions

The current work investigated the durability performance of a new non-proprietary UHPC mixture incorporating the ECat (which is a by-product originated by the oil refinery industry) as an internal curing agent. Based on the results presented in this paper, and the review on other commercial and non-proprietary UHPC/UHPFRC investigations, the following conclusions can be drawn:

- The total porosity evaluated by MIP at 28 days was 9.94%, which is slightly above the 75th percentile of results found in literature (8%). However, of the 9.94% total porosity only 0.51% lies in the range of the capillary porosity, which is the more critical in terms of durability performance. As expected, the total porosity decreased when extending the curing time (7.15% for 90 days).
- Both the average sorptivity (0.111 kg/($m^2 \times h^{0.5}$)) and the average non-steady state chloride migration coefficient (2.01 $\times$ 10^{-12} m^2/s), obtained at 28 days, lie in between the 25th and 75th percentiles of results found in literature for other UHPC.
- No carbonation could be detected on the tested UHPC specimens after 12 months in the accelerated carbonation chamber.
- No deleterious expansion due to alcalis-silica reaction or external sulphates attack is anticipated on the UHPC under study.

Major finding in this investigation is the belief reinforcement that the use of ECat as an internal curing agent in UHPC is feasible, particularly in mixtures for rehabilitation/strengthening purposes that require low early-ages cracking risk and on-site fabrication under normal casting and curing conditions.

CRediT authorship contribution statement

Ana Mafalda Matos: Investigation, Resources, Validation, Data curation, Writing – original draft. **Sandra Nunes:** Conceptualization, Methodology, Formal analysis, Visualization, Writing - review & editing, Supervision, Project administration, Funding acquisition. **Carla Costa:** Conceptualization, Methodology, Formal analysis, Visualization, Writing - review & editing. **José L. Barroso Aguiar:** Supervision, Funding acquisition.

Declaration of Competing Interest

The authors declare that they have no known competing financial interests or personal relationships that could have appeared to influence the work reported in this paper.

Acknowledgements

This work was financially supported by: Base Funding - UIDB/04708/2020 and Programmatic Funding – UIDP/04708/2020 of the CONSTRUCT – Instituto de I&D em Estruturas e Construções – funded by national funds through the FCT/MCTES (PIDDAC); by the project POCI-01-0145-FEDER-031777 – "UHPGRADE – Next generation of ultra-high performance fibre-reinforced cement-based composites for rehabilitation and strengthening of the existing infrastructure" funded by FEDER funds through COMPETE2020 – Programa Operacional Competitividade e Internacionalização (POCI) and by national funds (PIDDAC) through FCT/MCTES; and by FCT – Fundação para a Ciência e a Tecnologia through the PhD scholarship PD/BD/113636/2015, attributed within the Doctoral Program in Eco-Efficient Construction and Rehabilitation (EcoCoRe). Collaboration and materials supply by Sines Refinery/Galp Energia, Secil, Omya Comital, Sika and EUROMODAL is gratefully acknowledged.

Appendix A. Supplementary data

Supplementary data to this article can be found online at https://doi.org/10.1016/j.conbuildmat.2021.124681.

References

[1] C. Shi, Z. Wu, J. Xiao, D. Wang, Z. Huang, Z. Fang, A review on ultra high performance concrete: Part I. Raw materials and mixture design, Constr. Build. Mater. 101 (2015) 741–751, https://doi.org/10.1016/j.conbuildmat.2015.10.088.
[2] S. Abbas, M.L. Nehdi, M.A. Saleem, Ultra-high performance concrete: mechanical performance, durability, sustainability and implementation challenges, Int. J. Concr. Struct. Mater. 10 (3) (2016) 271–295, https://doi.org/10.1007/s40069-016-0157-4.
[3] D.Y. Yoo, N. Banthia, Mechanical properties of ultra-high-performance fiber-reinforced concrete: a review, Cem. Concr. Compos. 73 (2016) 267–280, https://doi.org/10.1016/j.cemconcomp.2016.08.001.
[4] J. Li, Z. Wu, C. Shi, Q. Yuan, Z. Zhang, Durability of ultra-high performance concrete – a review, Constr. Build. Mater. 255 (2020) 119296, https://doi.org/10.1016/j.conbuildmat.2020.119296.
[5] E. Cuenca, A. Mezzena, L. Ferrara, Synergy between crystalline admixtures and nano-constituents in enhancing autogenous healing capacity of cementitious composites under cracking and healing cycles in aggressive waters, Constr. Build. Mater. 266 (2021) 121447, https://doi.org/10.1016/j.conbuildmat.2020.121447.
[6] E. Cuenca, L. D'Ambrosio, D. Lizunov, A. Tretjakov, O. Volobujeva, L. Ferrara, Mechanical properties and self-healing capacity of ultra high performance fibre reinforced concrete with alumina nano-fibres: tailoring ultra high durability concrete for aggressive exposure scenarios, Cem. Concr. Compos. 118 (2021) 103956, https://doi.org/10.1016/j.cemconcomp.2021.103956.
[7] E. Cuenca, S. Rigamonti, E. Gastaldo Brac, L. Ferrara, Crystalline admixture as healing promoter in concrete exposed to chloride-rich environments: experimental study, J. Mater. Civ. Eng. 33 (3) (2021) 04020491, https://doi.org/10.1061/(ASCE)MT.1943-5533.0003604.
[8] E. Cuenca, P. Serna, Autogenous self-healing capacity of early-age ultra-high-performance fiber-reinforced concrete, Sustainability. 13 (2021) 3061, https://doi.org/10.3390/su13063061.
[9] M. Abid, X. Hou, W. Zheng, R.R. Hussain, High temperature and residual properties of reactive powder concrete – a review, Constr. Build. Mater. 147 (2017) 339–351, https://doi.org/10.1016/j.conbuildmat.2017.04.083.
[10] J.-J. Park, D.-Y. Yoo, S. Kim, S.-W. Kim, Benefits of synthetic fibers on the residual mechanical performance of UHPFRC after exposure to ISO standard fire, Cem. Concr. Compos. 104 (2019) 103401, https://doi.org/10.1016/j.cemconcomp.2019.103401.
[11] F. Toutlemonde, J. Resplendino, eds., Field Experience of UHPFRC Durability in an Air Cooling Tower, John Wiley & Sons, Inc., 2011. https://doi.org/10.1002/9781118557839.
[12] E. Brühwiler, E. Denarié, Rehabilitation and strengthening of concrete structures using ultra-high performance fibre reinforced concrete, Struct. Eng. Int. 23 (4) (2013) 450–457, https://doi.org/10.2749/101686613X13627347100437.
[13] S. Pyo, H.K. Kim, Fresh and hardened properties of ultra-high performance concrete incorporating coal bottom ash and slag powder, Constr. Build. Mater. 131 (2017) 459–466, https://doi.org/10.1016/j.conbuildmat.2016.10.109.
[14] A. Rajasekar, K. Arunachalam, M. Kottaisamy, V. Saraswathy, Durability characteristics of Ultra High Strength concrete with treated sugarcane bagasse ash, Constr. Build. Mater. 171 (2018) 350–356, https://doi.org/10.1016/j.conbuildmat.2018.03.140.

[15] V. Vaitkevičius, E. Šerelis, H. Hilbig, The effect of glass powder on the microstructure of ultra high performance concrete, Constr. Build. Mater. 68 (2014) 102–109, https://doi.org/10.1016/j.conbuildmat.2014.05.101.

[16] N.A. Soliman, A. Tagnit-Hamou, Partial substitution of silica fume with fine glass powder in UHPC: Filling the micro gap, Constr. Build. Mater. 139 (2017) 374–383, https://doi.org/10.1016/j.conbuildmat.2017.02.084.

[17] N. Van Tuan, G. Ye, K. van Breugel, A.L.A. Fraaij, D.D. Bui, The study of using rice husk ash to produce ultra high performance concrete, Constr. Build. Mater. 25 (4) (2011) 2030–2035, https://doi.org/10.1016/j.conbuildmat.2010.11.046.

[18] K. Wille, C. Boisvert-Cotulio, Material efficiency in the design of ultra-high performance concrete, Constr. Build. Mater. 86 (2015) 33–43, https://doi.org/10.1016/j.conbuildmat.2015.03.087.

[19] A. Arora, Y. Yao, B. Mobasher, N. Neithalath, Fundamental insights into the compressive and flexural response of binder- and aggregate-optimized ultra-high performance concrete (UHPC), Cem. Concr. Compos. 98 (2019) 1–13, https://doi.org/10.1016/j.cemconcomp.2019.01.015.

[20] P.P. Li, Q.L. Yu, H.J.H. Brouwers, Effect of coarse basalt aggregates on the properties of Ultra-high Performance Concrete (UHPC), Constr. Build. Mater. 170 (2018) 649–659, https://doi.org/10.1016/j.conbuildmat.2018.03.109.

[21] W. Meng, K.H. Khayat, Effect of graphite nanoplatelets and carbon nanofibers on rheology, hydration, shrinkage, mechanical properties, and microstructure of UHPC, Cem. Concr. Res. 105 (2018) 64–71, https://doi.org/10.1016/J.CEMCONRES.2018.01.001.

[22] T. Chen, X. Gao, M. Ren, Effects of autoclave curing and fly ash on mechanical properties of ultra-high performance concrete, Constr. Build. Mater. 158 (2018) 864–872, https://doi.org/10.1016/j.conbuildmat.2017.10.074.

[23] V.T.A. Van, C. Rößler, D.D. Bui, H.M. Ludwig, Rice husk ash as both pozzolanic admixture and internal curing agent in ultra-high performance concrete, Cem. Concr. Compos. 53 (2014) 270–278, https://doi.org/10.1016/j.cemconcomp.2014.07.015.

[24] H. Yazıcı, H. Yiğiter, A.Ş. Karabulut, B. Baradan, Utilization of fly ash and ground granulated blast furnace slag as an alternative silica source in reactive powder concrete, Fuel 87 (12) (2008) 2401–2407, https://doi.org/10.1016/j.fuel.2008.03.005.

[25] H. Yazıcı, M.Y. Yardımcı, H. Yiğiter, S. Aydın, S. Türkel, Mechanical properties of reactive powder concrete containing high volumes of ground granulated blast furnace slag, Cem. Concr. Compos. 32 (8) (2010) 639–648, https://doi.org/10.1016/j.cemconcomp.2010.07.005.

[26] F. Ferella, I. D'Adamo, S. Leone, V. Innocenzi, I. De Michelis, F. Vegliò, Spent FCC E-Cat: Towards a circular approach in the oil refining industry, Sustain. 11 (1) (2019) 113, https://doi.org/10.3390/su11010113.

[27] F. Ferella, V. Innocenzi, F. Maggiore, Oil refining spent catalysts: a review of possible recycling technologies, Resour. Conserv. Recycl. 108 (2016) 10–20, https://doi.org/10.1016/j.resconrec.2016.01.010.

[28] E. Restrepo, F. Vargas, E. López, C. Baudín, The potential of La-containing spent catalysts from fluid catalytic cracking as feedstock of mullite based refractories, J. Eur. Ceram. Soc. 40 (15) (2020) 6162–6170, https://doi.org/10.1016/j.jeurceramsoc.2020.04.051.

[29] Y. Zhou, S. Schulz, L.F. Lindoy, H. Du, S. Zheng, M. Wenzel, J.J. Weigand, Separation and recovery of rare earths by in situ selective electrochemical oxidation and extraction from spent fluid catalytic cracking (FCC) catalysts, Hydrometallurgy 194 (2020) 105300, https://doi.org/10.1016/j.hydromet.2020.105300.

[30] Fluid Catalytic Cracking Market Size | Global FCC Industry Report, 2025, (n.d.). https://www.grandviewresearch.com/industry-analysis/fluid-catalytic-cracking-fcc-market (accessed February 17, 2021).

[31] L.-P. Nguyen, Y.T.H. Pham, P.T. Ngo, T.V. Tran, L.V. Tran, N.T.H. Le, L.H. Nguyen, T.T. Dang, D.A. Nguyen, M. Wenzel, D. Hartmann, K. Gloe, J.J. Weigand, K. Kretschmer, Production of high purity rare earth mixture from iron-rich spent fluid catalytic cracking (FCC) catalyst using acid leaching and two-step solvent extraction process, Korean J. Chem. Eng. 35 (5) (2018) 1195–1202, https://doi.org/10.1007/s11814-018-0022-z.

[32] B. Alonso-Fariñas, M. Rodríguez-Galán, C. Arenas, F. Arroyo Torralvo, C. Leiva, Sustainable management of spent fluid catalytic cracking catalyst from a circular economy approach, Waste Manag. 110 (2020) 10–19, https://doi.org/10.1016/j.wasman.2020.04.046.

[33] C. Costa, J. Marques, Feasibility of Eco-Friendly Binary and Ternary Blended Binders Made of Fly-Ash and Oil-Refinery Spent Catalyst in Ready-Mixed Concrete Production, Sustain. 2018, Vol. 10, Page 3136. 10 (2018) 3136. https://doi.org/10.3390/SU10093136.

[34] A.M. Matos, S. Nunes, C. Costa, J.L. Barroso-Aguiar, Spent equilibrium catalyst as internal curing agent in UHPFRC, Cem. Concr. Compos. 104 (2019) 103362, https://doi.org/10.1016/j.cemconcomp.2019.103362.

[35] S. Nunes, C. Costa, Numerical optimization of self-compacting mortar mixture containing spent equilibrium catalyst from oil refinery, J. Clean. Prod. 158 (2017) 109–121, https://doi.org/10.1016/j.jclepro.2017.04.161.

[36] C. Costa, P. Marques, LOW-CARBON CEMENT WITH WASTE OIL-CRACKING CATALYST INCORPORATION By : Instituto de Telecomunicações / Instituto Superior de Engenharia de Lisboa, (2012) 3–11.

[37] C. Costa, M.S. Ribeiro, N. Brito, Effect of waste oil-cracking catalyst incorporation on durability of mortars, Mater. Sci. Appl. 05 (13) (2014) 905–914, https://doi.org/10.4236/msa:2014.513092.

[38] A.M. Matos, Design of Eco-efficient Ultra-high Performance Fibre Reinforced Cement-based Composite for Rehabilitation / Strengthening Applications, University of Porto, Faculty of Engineering, 2020.

[39] M. Canut, Pore structure and state of water in blended cement pastes, 2011.

[40] W. Wang, J. Liu, F. Agostini, C.A. Davy, F. Skoczylas, D. Corvez, Durability of an Ultra High Performance Fiber Reinforced Concrete (UHPFRC) under progressive aging, Cem. Concr. Res. 55 (2014) 1–13, https://doi.org/10.1016/j.cemconres.2013.09.008.

[41] D. Heinz, H.-M. Ludwig, Heat Treatment and the Risk of DEF Delayed Ettringite Formation in UHPC, in: M. Schmidt, E. Fehling, C. Geisenhanslüke (Eds.), Int. Symp. Ultra High Perform. Concr., Kassel, Germany, 2004.

[42] T. Teichmann, M. Schmidt, Influence of the packing density of fine particles on structure, strength and durability of {UHPC}, First Int. Symp. Ultra High Perform. Concr. {Kassel}. (2004) 313–323. https://www.researchgate.net/profile/Lesday_Martinez/publication/271196269_Lime-pozzolan_binder_as_a_very_fine_mineral_admixture_in_concrete/links/54bffe160cf28a6324a03408.pdf#page=329.

[43] A. Cwirzen, The effect of the heat-treatment regime on the properties of reactive powder concrete, Adv. Cem. Res. 19 (1) (2007) 25–33, https://doi.org/10.1680/adcr.2007.19.1.25.

[44] V.T. Nguyen, Rice husk ash as a mineral admixture for ultra high performance concrete, Technische Universiteit Delf (2011).

[45] J. Scheydt, H. Müller, Microstructure of ultra high performance concrete (UHPC) and its impact on durability, in: 3rd Int. Symp. Ultra High Perform. Concr., Kassel, Germany, 2012. https://www.google.com/books?hl=pt-PT&lr=&id=LufCDwJ-sacC&oi=fnd&pg=PA349&dq=Microstructure+of+ultra+high+performance+concrete+(UHPC)+and+its+impact+on+durability&ots=b3wNtRyM4q&sig=5xg-G4pLF6YsgOnnjyro6rFZjSQ (accessed February 15, 2017).

[46] E. Ghafari, H. Costa, E. Júlio, A. Portugal, L. Durães, The effect of nanosilica addition on flowability, strength and transport properties of ultra high performance concrete, Mater. Des. 59 (2014) 1–9, https://doi.org/10.1016/j.matdes.2014.02.051.

[47] R.S. Edwin, E. Gruyaert, J. Dils, N. De Belie, Influence of vacuum mixing on the carbonation resistance and microstructure of reactive powder concrete containing secondary copper slag as supplementary cementitious material (SCM), Procedia Eng. 171 (2017) 534–542, https://doi.org/10.1016/j.proeng.2017.01.367.

[48] W. Huang, H. Kazemi-Kamyab, W. Sun, K. Scrivener, Effect of replacement of silica fume with calcined clay on the hydration and microstructural development of eco-UHPFRC, Mater. Des. 121 (2017) 36–46, https://doi.org/10.1016/j.matdes.2017.02.052.

[49] Z. Wu, C. Shi, K.H. Khayat, Multi-scale investigation of microstructure, fiber pullout behavior, and mechanical properties of ultra-high performance concrete with nano-CaCO3 particles, Cem. Concr. Compos. 86 (2018) 255–265, https://doi.org/10.1016/j.cemconcomp.2017.11.014.

[50] W. Huang, H. Kazemi-Kamyab, W. Sun, K. Scrivener, Effect of cement substitution by limestone on the hydration and microstructural development of ultra-high performance concrete (UHPC), Cem. Concr. Compos. 77 (2017) 86–101, https://doi.org/10.1016/j.cemconcomp.2016.12.009.

[51] O.M. Abdulkareem, A. Ben Fraj, M. Bouasker, A. Khelidj, Effect of chemical and thermal activation on the microstructural and mechanical properties of more sustainable UHPC, Constr. Build. Mater. 169 (2018) 567–577, https://doi.org/10.1016/j.conbuildmat.2018.02.214.

[52] N.K. Lee, K.T. Koh, M.O. Kim, G.S. Ryu, Uncovering the role of micro silica in hydration of ultra-high performance concrete (UHPC), Cem. Concr. Res. 104 (2018) 68–79, https://doi.org/10.1016/j.cemconres.2017.11.002.

[53] V.T. NGUYỄN, Rice Husk Ash as a Mineral Admixture for Ultra High Performance Concrete, Technische Universiteit Delf, n.d.

[54] H. Beushausen, L. Fernandez Luco, Performance-Based Specifications and Control of Concrete Durability: State-of-the-Art Report RILEM TC 230-PSC, 2015. https://doi.org/10.1007/978-94-017-7309-6.

[55] G. Franke, L. Schmidt, H. Deckelmann, Behaviour of ultra high-performance concrete with respect to chemical attack, 2nd Symp, UHPC. (2008) 453–459, https://doi.org/10.1017/CBO9781107415324.004.

[56] E. Ghafari, H. Costa, E. Júlio, A. Portugal, L. Durães, Optimization of UHPC by adding nanomaterials, 3rd Int, Symp. UHPC Nanotechnol. High Perform. Constr. Mater. (2012) 71–78.

[57] S. Abbas, A.M. Soliman, M.L. Nehdi, Exploring mechanical and durability properties of ultra-high performance concrete incorporating various steel fiber lengths and dosages, Constr. Build. Mater. 75 (2015) 429–441, https://doi.org/10.1016/J.CONBUILDMAT.2014.11.017.

[58] A. Tafraoui, G. Escadeillas, T. Vidal, Durability of the Ultra High Performances Concrete containing metakaolin, Constr. Build. Mater. 112 (2016) 980–987, https://doi.org/10.1016/j.conbuildmat.2016.02.169.

[59] H. Huang, X. Gao, H. Wang, H. Ye, Influence of rice husk ash on strength and permeability of ultra-high performance concrete, Constr. Build. Mater. 149 (2017) 621–628, https://doi.org/10.1016/J.CONBUILDMAT.2017.05.155.

[60] R. Wang, X. Gao, Q. Li, Y. Yang, Influence of splitting load on transport properties of ultra-high performance concrete, Constr. Build. Mater. 171 (2018) 708–718, https://doi.org/10.1016/j.conbuildmat.2018.03.174.

[61] A. Arora, A. Almujaddidi, F. Kianmofrad, B. Mobasher, N. Neithalath, Material design of economical ultra-high performance concrete (UHPC) and evaluation of their properties, Cem. Concr. Compos. 104 (2019) 103346, https://doi.org/10.1016/j.cemconcomp.2019.103346.

[62] L. Tang, L.-O. Nilsson, P.A.M. Basheer, Resistance of Concrete to Chloride Ingress: Testing and modelling, 2011.

[63] S. Teng, V. Afroughsabet, C.P. Ostertag, Flexural behavior and durability properties of high performance hybrid-fiber-reinforced concrete, Constr. Build. Mater. 182 (2018) 504–515, https://doi.org/10.1016/j.conbuildmat.2018.06.158.

[64] Y. Chen, R. Yu, X. Wang, J. Chen, Z. Shui, Evaluation and optimization of Ultra-High Performance Concrete (UHPC) subjected to harsh ocean environment:

towards an application of Layered Double Hydroxides (LDHs), Constr. Build. Mater. 177 (2018) 51–62, https://doi.org/10.1016/J.CONBUILDMAT.2018.03.210.
[65] J.M. Gandiá-Romero, J.E. Ramón-Zamora, I. Gasch, M. Valcuende, V. Calvet, R. Calabuig, P. Serna, Absorption, porosity, capillarity and chloride diffusion in ultra high performance concretes, 6th Int, Conf. Durab. Concr. Struct. ICDCS 2018 (2018) 303–308.
[66] P.R.; Spiesz, M. Hunger, Towards a more common use of Ultra-High Performance Concrete (UHPC) – development of UHPC for ready-mix and prefabrication concrete plants, 11th High Perform. Concr. Conf. HPC Tromso 2017. (2017) 1–10. https://pure.tue.nl/ws/files/58624276/46_UHPC_Przemek_Spiesz.pdf.
[67] S.H. Ghasemzadeh Mosavinejad, M.A.M. Langaroudi, J. Barandoust, A. Ghanizadeh, Electrical and microstructural analysis of UHPC containing short PVA fibers, Constr. Build. Mater. 235 (2020) 117448, https://doi.org/10.1016/j.conbuildmat.2019.117448.
[68] E.P. Nielsen, C.M.Q. Batista, J.S. Damtoff, Sustainable high and ultra-high performance concrete. The next generation binders., 2020. https://www.aalborgwhite.com/sites/default/files/documents/2020-04/White Paper_Sustainable High and Ultra High Performance Concrete – the next generation binders.pdf.
[69] I. Ferdosian, Material Development and Self-healing Capacity of Eco-Efficient Ultra-High Performance Concrete (EEUHPC), Universidade do Minho Escola de Engenharia, 2016.
[70] M. Schmidt, E. Fehling, Ultra-high-performance concrete: Research, development and application in Europe, Seventh Int. Symp. Util. High Strength/High-Performance Concr. (2005) 51–78. http://download.contec-aps.com/uploads/tx_mpdownloadcenter/pp_fp_2005_003_eng_01.pdf.
[71] N. Roux, C. Andrade, M.A. Sanjuan, EXPERIMENTAL STUDY OF DURABILITY OF REACTIVE POWDER CONCRETES By N. Roux,t C. Andrade,z and M. A. Sanjuan 3, J. Mater. Civ. Eng. 8 (1996) 1–6.
[72] J. Liu, S. Song, L. Wang, Durability and micro-structure of reactive powder concrete, J. Wuhan Univ. Technol. Mater. Sci. Ed. 24 (3) (2009) 506–509, https://doi.org/10.1007/s11595-009-3506-1.
[73] C. Andrade, J. Torres, Long term carbonation of UHPC, in: RILEM-Fib-AFGC Int. Symp. Ultra-High Perform. Fibre-Reinforced Concr. UHPFRC 2013, 2013: pp. 249–256.
[74] J. Piérard, B. Dooms, N. Cauberg, Durability evaluation of different types of UHPC, RILEM-Fib-AFGC Int. Symp. Ultra-High Perform. Fibre-Reinforced Concr. UHPFRC 2013 –. (2013) 275–284. http://demo.webdefy.com/rilem-new/wp-content/uploads/2016/10/f44eafb7c62b85f77bb95f4880434a80.pdf.
[75] B. Graybeal, J. Tanesi, Durability of an ultrahigh-performance concrete, J. Mater. Civ. Eng. 19 (10) (2007) 848–854, https://doi.org/10.1061/(ASCE)0899-1561(2007)19:10(848).
[76] B. Möser, C. Pfeifer, J. Stark, Durability and microstructural development during hydration in ultra-high performance concrete, Concr. Repair, Rehabil. Retrofit. II - Proc. 2nd Int. Conf. Concr. Repair, Rehabil. Retrofit. ICCRRR. (2009) 87–88. https://doi.org/10.1201/9781439828403.ch11.
[77] N.A. Soliman, A. Tagnit-Hamou, Using glass sand as an alternative for quartz sand in UHPC, Constr. Build. Mater. 145 (2017) 243–252, https://doi.org/10.1016/j.conbuildmat.2017.03.187.
[78] J. Sawab, I. Lim, Y.L. Mo, M. Li, H. Wang, M. Guimaraes, Ultra-high-performance concrete and advanced manufacturing methods for modular construction, 2016.
[79] S. Ahmad, I. Hakeem, M. Maslehuddin, Development of an optimum mixture of ultra-high performance concrete, Eur. J. Environ. Civ. Eng. 20 (9) (2016) 1106–1126, https://doi.org/10.1080/19648189.2015.1090925.
[80] M.L. Chuang, W.H. Huang, Durability analysis testing on reactive powder concrete, Adv. Mater. Res. 811 (2013) 244–248, https://doi.org/10.4028/www.scientific.net/AMR.811.244.
[81] J. Piérard, B. Dooms, N. Cauberg, Evaluation of durability parameters of UHPC using accelerated lab tests, Proc. 3rd Int. Symp. UHPC Nanotechnol. High Perform. Constr. Mater. Kassel, Ger. (2012) 371–376. https://books.google.com/books?hl=en&lr=&id=LufCDwJ-sacC&oi=fnd&pg=PA371&dq=Piérard,+J.,+Dooms,+B.,+and+Cauberg,+N.,+"Evaluation+of+Durability+Parameters+of+UHPC+Using+Accelerated+Lab+Tests,"+Proceedings+of+Hipermat+2012+3rd+Internati.
[82] A.S. El-Dieb, Mechanical, durability and microstructural characteristics of ultra-high-strength self-compacting concrete incorporating steel fibers, Mater. Des. 30 (10) (2009) 4286–4292, https://doi.org/10.1016/j.matdes.2009.04.024.
[83] J. Zhang, G.W. Scherer, Comparison of methods for arresting hydration of cement, Cem. Concr. Res. 41 (10) (2011) 1024–1036, https://doi.org/10.1016/j.cemconres.2011.06.003.
[84] K. Scrivener, R. Snellings, B. Lothenbach, A Practical Guide to Microstructural Analysis of Cementitious Materials, 2018. https://doi.org/10.1201/b19074.
[85] S. Diamond, The microstructure of cement paste and concrete – a visual primer, Cem. Concr. Compos. 26 (8) (2004) 919–933, https://doi.org/10.1016/j.cemconcomp.2004.02.028.
[86] R.S. Edwin, M. Mushthofa, E. Gruyaert, N. De Belie, Quantitative analysis on porosity of reactive powder concrete based on automated analysis of back-scattered-electron images, Cem. Concr. Compos. 96 (2019) 1–10, https://doi.org/10.1016/j.cemconcomp.2018.10.019.
[87] T. Zhang, O.E. Gjorv, Diffusion behaviour of chloride ions in concrete, Cem. Concr. Res. 26 (1996) 907–917.